Atria Dilla, D., Anggraini, A., Nukman, M., Lühr, B., Suryanto, W. (2019): Velocity structure of the earthquake zone of the M6.3 Yogyakarta earthquake 2006 from a seismic tomography study. - *Geophysical Journal International*, *216*, 1, pp. 439—452.

DOI: http://doi.org/10.1093/gji/ggy430

Geophysical Journal International

Geophys. J. Int. (2019) **216,** 439–452
Advance Access publication 2018 October 16
GJI Seismology

doi: 10.1093/gji/ggy430

Velocity structure of the earthquake zone of the M6.3 Yogyakarta earthquake 2006 from a seismic tomography study

Atria Dilla Diambama,[1] Ade Anggraini,[1] Mochamad Nukman,[1] Birger-Gottfried Lühr[2] and Wiwit Suryanto[1]

[1] *Seismology Research Group, Department of Physics, Universitas Gadjah Mada Yogyakarta, Sekip Utara* 55281*, Indonesia. E-mail: ws@ugm.ac.id*
[2] *Department of Physics of Earth, GFZ German Research Centre for Geosciences, Telegrafenberg,* 14473 *Potsdam, Germany*

Accepted 2018 October 15. Received 2018 October 5; in original form 2017 August 22

SUMMARY

On 2006 May 26 at 23:54 UTC, a moderate shallow crustal earthquake with a moment magnitude of 6.3 occurred in the southern part of Yogyakarta in Java, Indonesia. The earthquake caused severe damages in the area in addition to over 5700 casualties. The cause of this earthquake was initially believed to have been a rupture on the northeast–southwest trending Opak Fault; however, the role of this fault in the earthquake continues to be debated. Therefore, this study presents a subsurface model constructed to characterize the fault geometry associated with the earthquake. We used previously reported aftershock data to image subsurface velocity variations through seismic tomographic inversion of primary waves, shear waves and their velocity ratio (V_p/V_s). Using data from 10 stations around the hypothetical fault, 588 aftershock events were mostly located 10–15 km east of the Opak River Fault with a maximum depth of approximately 20 km. The seismic tomographic inversion results indicated that severe damage during the earthquake occurred in areas with larger V_p/V_s ratios associated with unconsolidated sediments, in accordance with previous findings. Furthermore, the configuration of an unnamed fault that was activated during the earthquake is delineated by a velocity anomaly with a depth of up to 5–7 km. This structure is interpreted as a strike-slip fault with a reverse component dipping to the east, striking northeast–southwest.

Key words: Seismic tomography; earthquake; Yogyakarta; Strike-slip fault.

1 INTRODUCTION

The activity of Opak Fault has been considered to be the major controller of the Yogyakarta earthquake 2006 (Karnawati *et al.* 2007; Walter *et al.* 2008). The current stress (North–South trend) from the subduction of Indo-Australian against Eurasia plates is controlled by the deformation pattern along Java, where the Opak Fault of Yogyakarta lies in the central segment (Rahardjo *et al.* 1995). The kinematic of the Opak Fault is still debatable, but it is considered to be a left-lateral fault (Tsuji *et al.* 2009). On 2006 May 27 at 05:54 a.m. local time, an earthquake occurs with a moment magnitude (M_w) of 6.3 in the vicinity of the Opak Fault. Although the magnitude of this earthquake was moderate, the shallow depth (approximately 21 km) and onshore location of the events resulted in numerous casualties and destruction of heritage buildings, with a larger societal impact. Ultimately, nearly 6000 people died, 37 000 were injured, more than 240 000 houses were destroyed and more than 600 000 people were displaced from their homes, with total economic losses of around USD 3.1 billion (International Recovery Platform & Universitas Gadjah Mada 2009).

The aftershock activity was recorded by a rapid response team from the German Task Force for Earthquakes (GTF, coordinated by GFZ Potsdam) along with the Indonesian Meteorological Agency (BMKG), while Universitas Gadjah Mada (UGM) installed the first seismometer network on 2006 May 31. A temporary network consisting of 12 short-period seismometers was setup and has been operating since its initiation on 2006 May 31. The network layout includes the earthquake disaster area around the Opak Fault, which was expected to experience intense aftershock activity. Another team from Japan also conducted a field study focusing on the deformation around the Opak Fault utilizing satellite radar imaging (Tsuji *et al.* 2009). The Japanese team hypothesized that the earthquake rupture fault trace was parallel to the Opak Fault and bent significantly towards its southern termination. Furthermore, Walter *et al.* (2008) concluded that the soft volcanic deposits filling the Yogyakarta graben bound by the Opak Fault amplified the ground motion, which resulted in heavy damage to the southern part of Yogyakarta and areas along the Opak Fault.

Previous studies indicate that the earthquake hypocentre was located near the Opak Fault zone as reported by different agencies

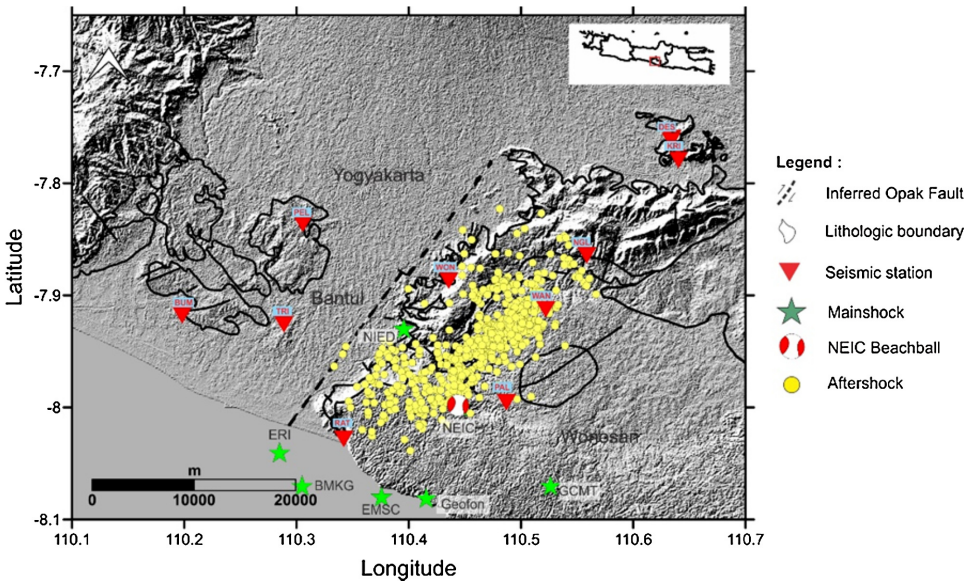

Figure 1. Mainshock epicentre of 2006 Yogyakarta earthquake (green star) as reported by different agencies and aftershocks recorded by temporary seismic network (Anggraini 2013). Seismic station locations are marked by red triangles. The yellow dots show the distribution of all local earthquakes. The locations of the vertical tomographic sections are marked by orange lines.

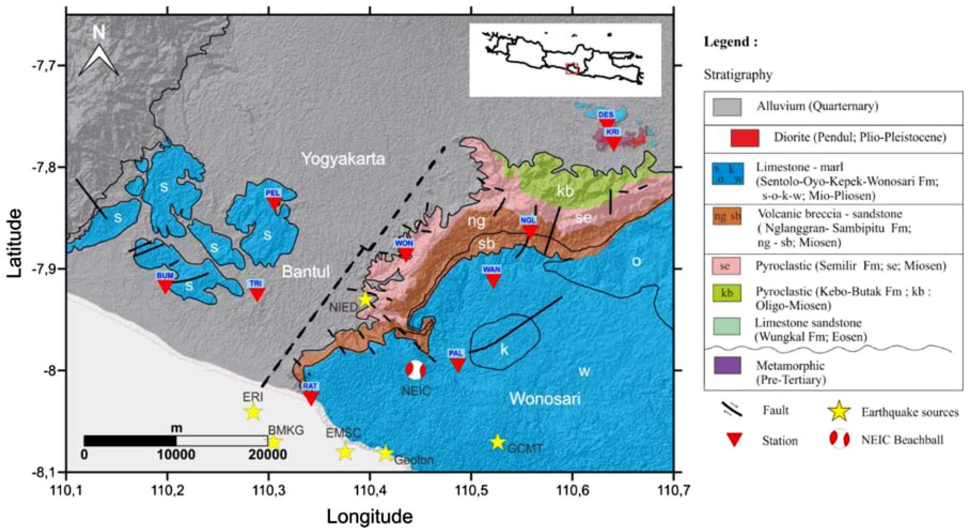

Figure 2. Geological and structural map of Yogyakarta (Rahardjo *et al.* 1995). The thick dashed line represents the Opak Fault. The stars represent the hypocentre location of Yogyakarta earthquake from different agencies (Anggraini 2013).

(Wagner *et al.* 2007; Anggraini 2013). In fact, the hypocentre locations lied off the fault as shown in Fig. 1. Furthermore, analysis of the recorded aftershocks demonstrated that the hypocentres were not located directly on this fault but were shifted 10–15 km to the east (Walter *et al.* 2008). An advanced investigation from waveform modelling, Kawazoe & Koketsu (2010) finds that two segments may have ruptured into a left-lateral strik-slip fault close to the Opak Fault and a reverse dip–slip fault to the southwest. Therefore, until recently, the fault location and geometry have been subjects of several intensive studies.

This paper aimed to establish more detailed subsurface velocity imagery of the 2006 Yogyakarta earthquake zone through a tomography study based on primary (*P* wave) and secondary wave (*S* wave) arrival times. Tomographic imaging at local scale has not been previously performed, especially for the area in and around the 2006 earthquake zone. More regional tomography studies have been carried out by earlier researchers, that is, Koulakov *et al.* (2007) and Wagner *et al.* (2007). They observe a clear south-to-north V_p/V_s anomaly contrast between higher and lower values that passes through the epicentre of the 2006 earthquake, which may

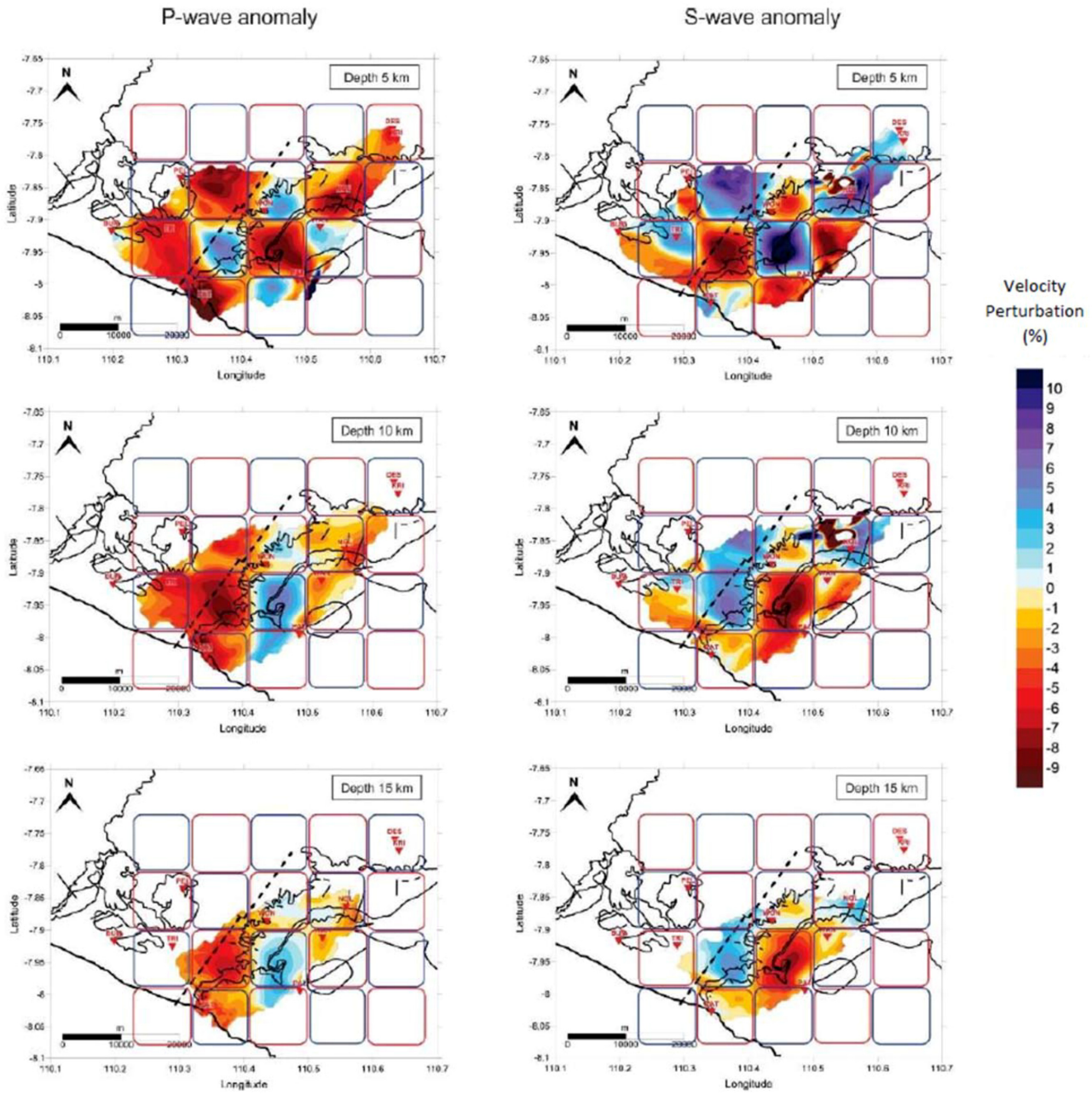

Figure 3. The result of *P*- and *S*-wave checkerboard anomaly test in horizontal sections, with 10 × 10 km^2 grid size. The colour-scale values are velocity perturbations relative to the 1-D velocity model in per cent (per cent) for 5, 10 and 15 km slice depth, for *P*- (left-hand side) and *S*-wave (right-hand side).

represent a contact zone between two blocks with different petrophysical properties. However, detailed tomographic imagery cannot be obtained for this regional-scale experiment.

2 GEOLOGICAL SETTING

Yogyakarta is located in a N–S-oriented depression filled with Quaternary deposits, mostly consist of volcanic product of Merapi. The morphology of Yogyakarta depression and Wonosari High area is inherited from the inactive Oligo–Miocene volcanic arc formed by subduction between the Indo-Australian and Eurasian plates. This former volcanic arc is currently situated 30–40 km south of the modern volcanic arc. The eastern border of Yogyakarta depression and Wonosari High has been interpreted by the existence of an inferred fault (known as Opak Fault), striking northeast–southwest (Fig. 2) (Rahardjo *et al.* 1995).

The basement of the Southern Mountain range in the Yogyakarta–Wonosari area is composed of low-grade metamorphic rocks (Late Cretaceous age; Prasetyadi 2007), exposing at northeast of the research area. This basement is overlain by an Eocene limestone–sandstone sequence of the Wungkal Gamping Formation (Fm). The younger rock belongs to The Kebo Butak, Semilir and Nglanggran Formations, consisting of Oligo–Miocene volcanic rock sequences (with compositions basaltic–andesitic–pyroclastic) with a

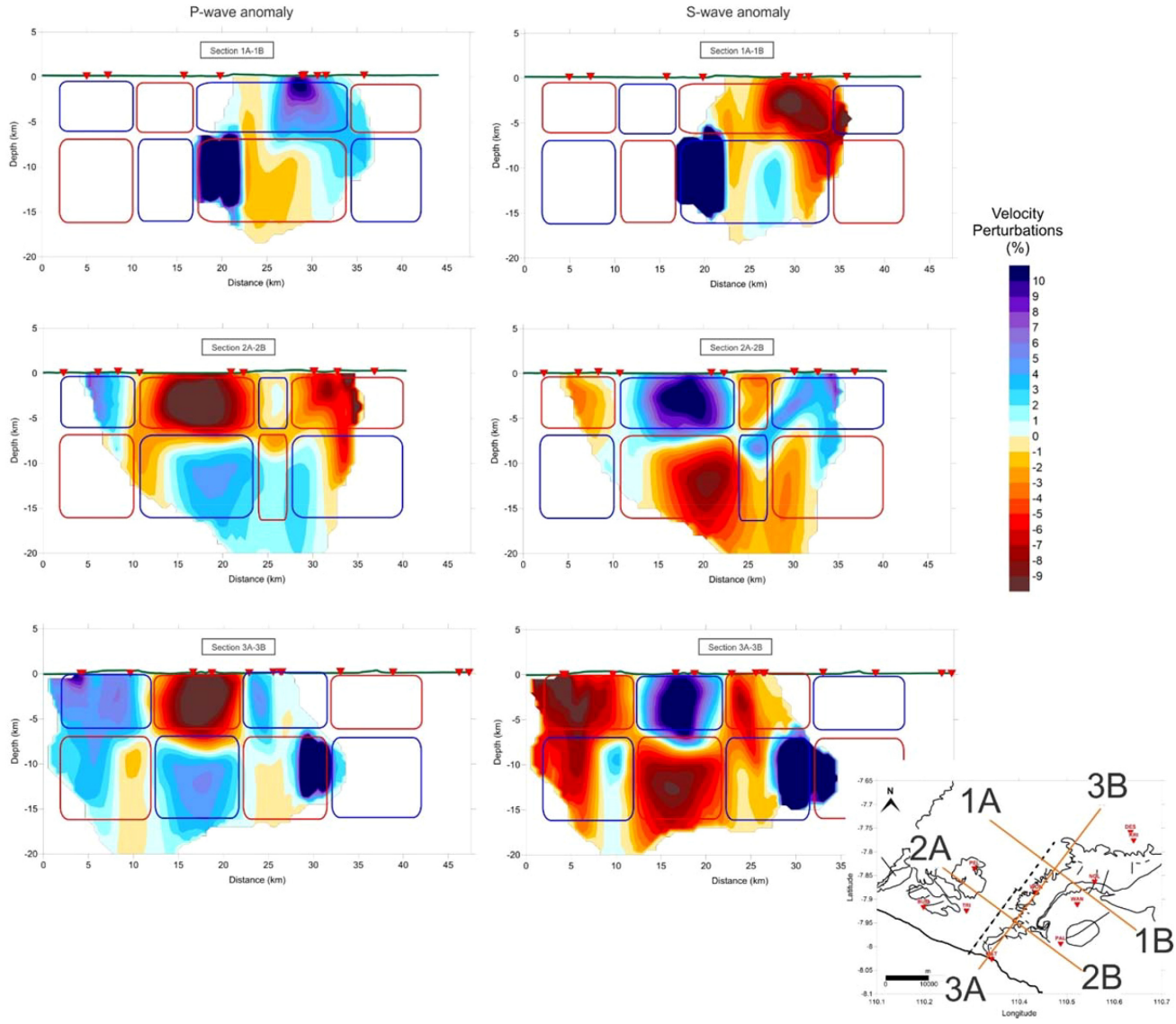

Figure 4. *P*- and *S*-wave checkerboard anomaly test results in vertical sections, with a grid of 10 × 10 km^2 and colour-scale values represent the high- and low-velocity anomalies of the synthetic model.

total thickness of up to 1600 m (Surono *et al.* 1992; Rahardjo *et al.* 1995). Basaltic rocks unit (diabase) intruded these volcanic formations dated at 33–24 Ma (Soeria-Atmadja *et al.* 1994; Setiawan pers. comm. 2018), and the typical of this intrusion rock is exposed at Pendul area (Bayat). Limestone unit with an approximate thickness of 960 m belonging to the Sentolo Fm, Oyo Fm, Wonosari Fm and the Kepek Fm (Rahardjo *et al.* 1995; Sudarno 1997) overly the older volcanic formations. In short, the distinct nature of the volcanic and carbonate rock types in the Southern Mountain area is expected to produce horizontally sharp velocity contrasts in the upper crust.

The regional north–south compressive stress direction controls the trends of fractures and faults in the upper crust across Java. The existing faults trend northwest–southeast (NE–SW) and northeast–southwest (NE–SW). The latter trend is morphologically expressed in a 30-km-long buried fault scarp in the Opak area. The reactivation of Opak Fault is believed to control the 2006 Yogyakarta earthquake.

3 DATA SET

The study area around the Opak Fault is located at 7°39′00′S–8°6′00′S and 110°6′00′E–110°42′00′E (Fig. 1), covering an area of approximately 65 × 50 km^2. The location of the seismic stations distributed around the Opak Fault are indicated by inverted red triangles in Fig. 1. Seven days following the earthquake, the setup of a temporary network of 10 seismic stations (type Mark L4–3D 1 Hz and Earth Data Logger EDL) was completed. In all stations, the

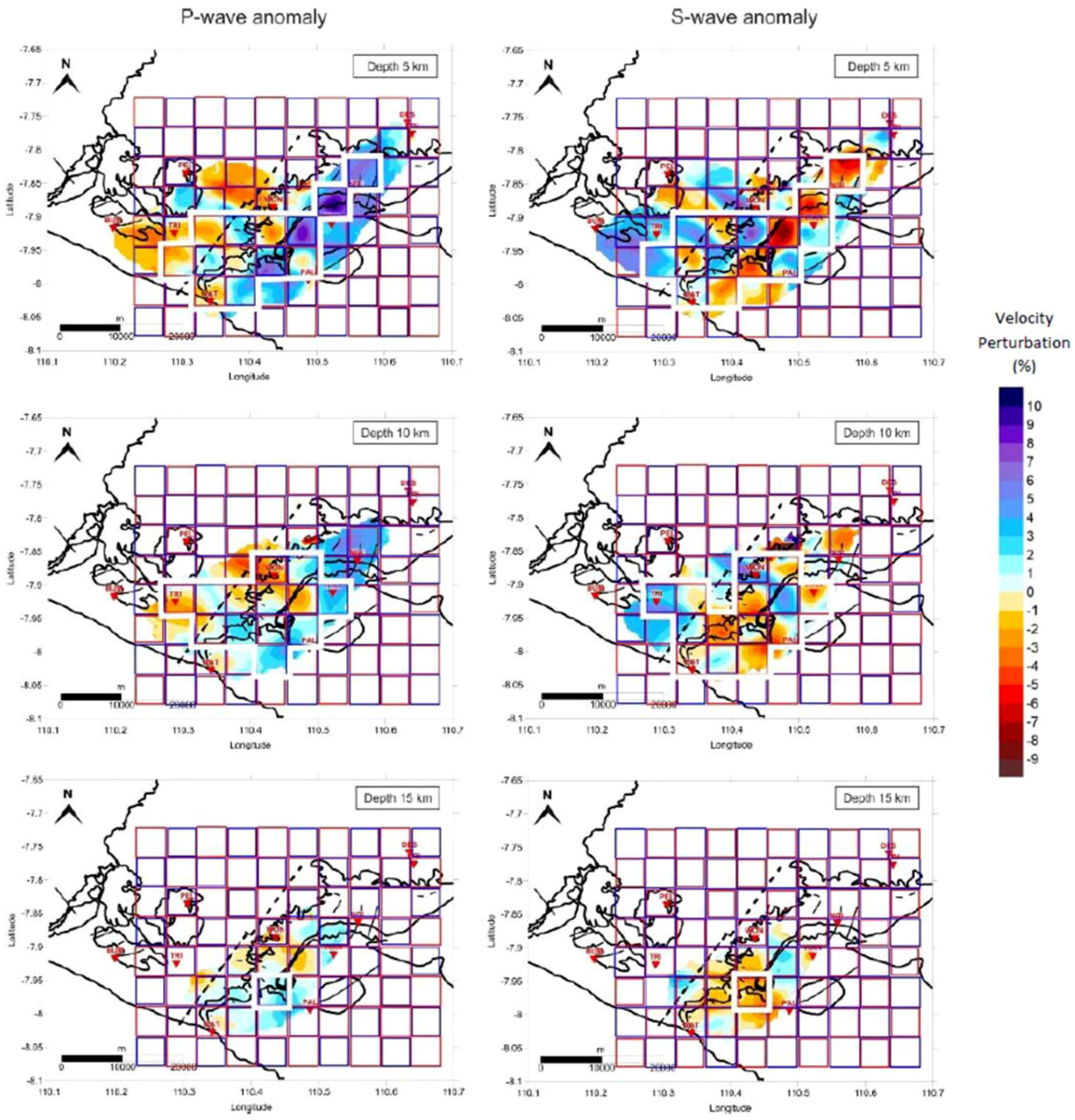

Figure 5. *P*- and *S*-wave checkerboard anomaly test results in horizontal sections, with a grid of 5 × 5 km^2 and colour-scale values represent the high- and low-velocity anomalies of the synthetic model. A good correlation area is shown on the white rectangular.

time was calibrated with an internal Global Positioning System time code signal. The average interstation distance was approximately 10 km, with around 4 km distance near the Opak River Fault and approximately 16 km between more distant stations.

This tomography study utilized aftershock data to determine the seismic velocity distribution in the study area and to highlight the subsurface geometry of the Opak Fault up to 30 km depth. The aftershock events used for this research were the previously located hypocenters based on manually picked *P*- and *S*-waves arrival time and relocated by earlier researchers (Walter *et al.* 2008; Anggraini 2013). The catalogue contains events ranging in magnitude from M_L 0.02–3.55 whereas majority of the aftershocks are observed over a depth range of 4–17 km. The average hypocentre error for this data set is ±800 m in the lateral direction and ±1200 m in the vertical direction (Anggraini 2013). And 588 events consisting of 3769 *P*-wave phases and 3407 *S*-wave phases were used in this study.

4 METHODS AND MODEL QUALITY

In this research, the data processing was performed using the updated version of LOTOS-13 (Local Tomographic Inversion Program) as described in Koulakov (2009). Several important parameters area were required to perform a tomographic inversion, including the arrival times of the *P*- and *S*-wave picking, hypocentre locations, the seismic station coordinates, the initial velocity model and the boundary of the study area. Seismic tomography was then conducted by comparing the observed arrival time of a seismic wave (recorded by seismometer) to the theoretical arrival time. The tomographic inversion was performed through five steps, that is, calculation of the reference traveltime

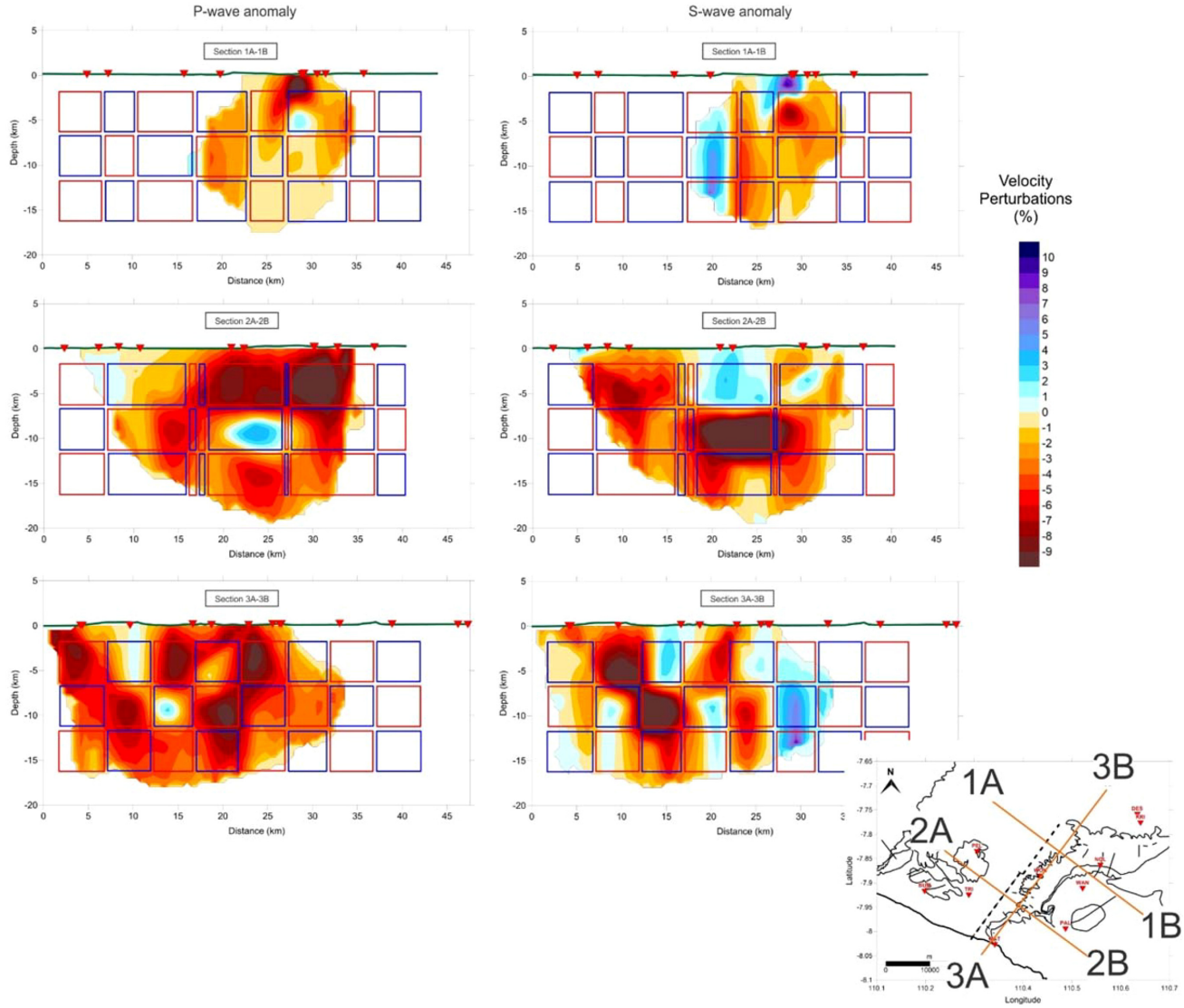

Figure 6. *P*- and *S*-wave checkerboard anomaly test results in vertical sections of Fig. 5. The colour-scale values represent the high- and low-velocity anomalies of the synthetic model.

table; the forward model computation of traveltime using bending method (Um & Thurber 1987); parameterisation of the velocity grid based on vertical lines distributed regularly in map view (e.g. with steps of 10 × 10 km), resulting an independent of the distribution of nodes/cells of the inversion result, that is, considered as a quasi-continuous parazonllymeterisation; matrix construction based on the obtained ray path; and simultaneously *P*- and *S*-velocity inversion (Wagner *et al.* 2007). The inversion was controlled by the number of iteration, the amplitude damping and the smoothing coefficient. LOTOS-13 was designed to find the optimum values of smoothing and amplitude damping based on synthetic modelling. The optimum value for the horizontal and vertical smoothing coefficient are 0.7 and 0.2, respectively. A more detailed methodology of the inversion strategies can be found in Koulakov (2009).

We used an initial velocity model from the earlier Merapi Amphibious Experiment Project (MERAMEX Project, Bohm *et al.* 2005) which was aimed to understand the volcanic system in the active continental margin in central Java. The same velocity model was also used by Wagner *et al.* (2007) to perform active and passive seismic tomography in central Java. This velocity model is used as input for LOTOS-13 program.

It is a standard to perform synthetic resolution test at the beginning of a tomography study to determine the confidence level of a volume of the tomogram obtained from the tomographic inversion result and based on the distribution of sources and stations. This tomography study focusses on the fault which is associated with the distribution of aftershock extending 20 km in NE–SW trend and 17 km depth. For this purpose, two cubic models (a checkerboard resolution test, CRT), i.e., 10 × 10 × 10 km^3 and 5 × 5 × 5 km^3, with a maximum depth of 30 km were tested. The CRT of 10 × 10 × 10 km^3 was adequate to model the targeted fault, while the 5 × 5 × 5 km^3 was used to test the higher resolution of the subsurface structure.

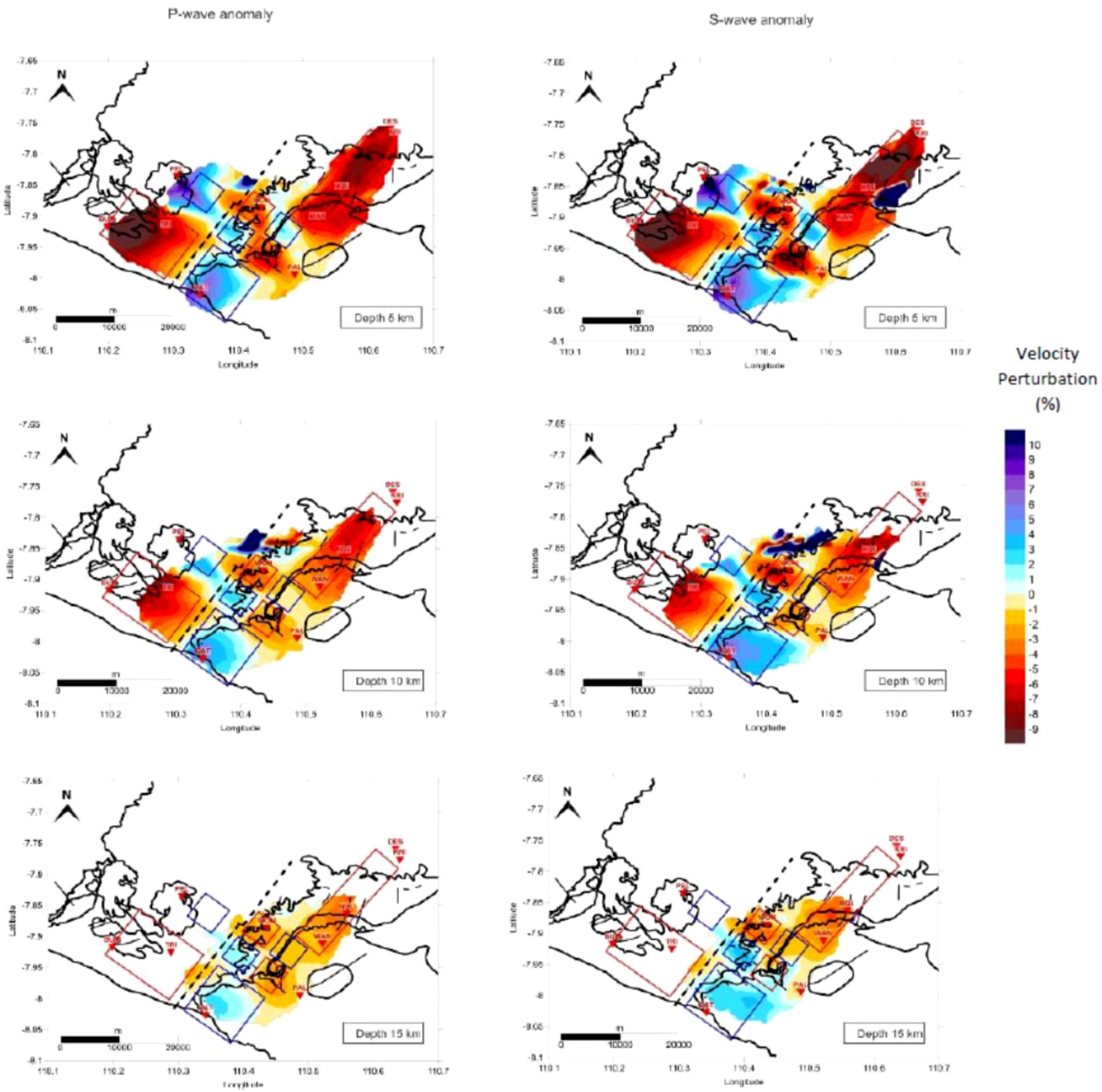

Figure 7. *P*- and *S*-wave resolution test results in horizontal sections, with 5 × 5 km^2 and 10 × 10 km^2 grid size with the red and blue rectangle represent the high- and low-velocity anomalies of the synthetic model.

The test was performed by applying the seismic rays from the sources to the stations and obtaining the total ray paths representing the tomogram boundary that can be found from the seismic events and station configurations. An CRT was conducted using the method described in Muksin *et al.* (2013) to verify the ray coverage data and to identify the maximum depth of good quality resolution with which to perform tomographic inversion, as the inversion result in areas of poor data resolution can negatively affect the resolution of the velocity distribution. Furthermore, this resolution test also indicated the spatial resolution of the tomogram image.

The raytracing algorithm is called bending tracing algorithm from Um and Thurber (1987) . LOTOS-13 uses a basic principle of bending algorithm that was performed in several steps to find a path with minimum traveltime. The initial step of the ray is a straight line. Then, to achieve the fixed position, the ray has to deform in some points along the ray path. The ray will choose to travel through high-velocity anomalies rather than low-velocity anomalies. This bending tracing algorithm is designed for 3-D case.

The next step to process the data was the iterative tomographic inversion. The initial step to run the inversion was determining the location of the sources using Goal Function equation which reflected the rough source position in 3-D space based on 1-D velocity model from active seismic experiment data by Wagner *et al.* (2007) in the south of Java.

The source coordinates were corrected on the basis of the rays using the bending method. Afterward, the 3-D velocity anomalies were linearly distributed in nodes in the study volume to interpolate

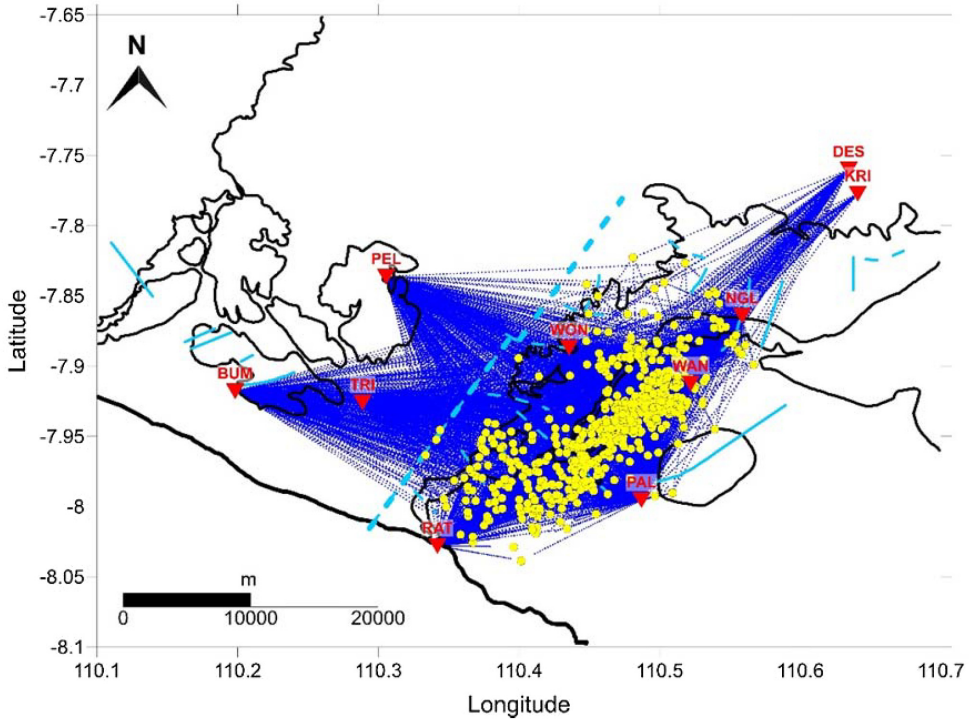

Figure 8. Ray coverage in horizontal section slices. Inverted triangles represent seismic stations, and yellow dots indicate earthquake hypocentres.

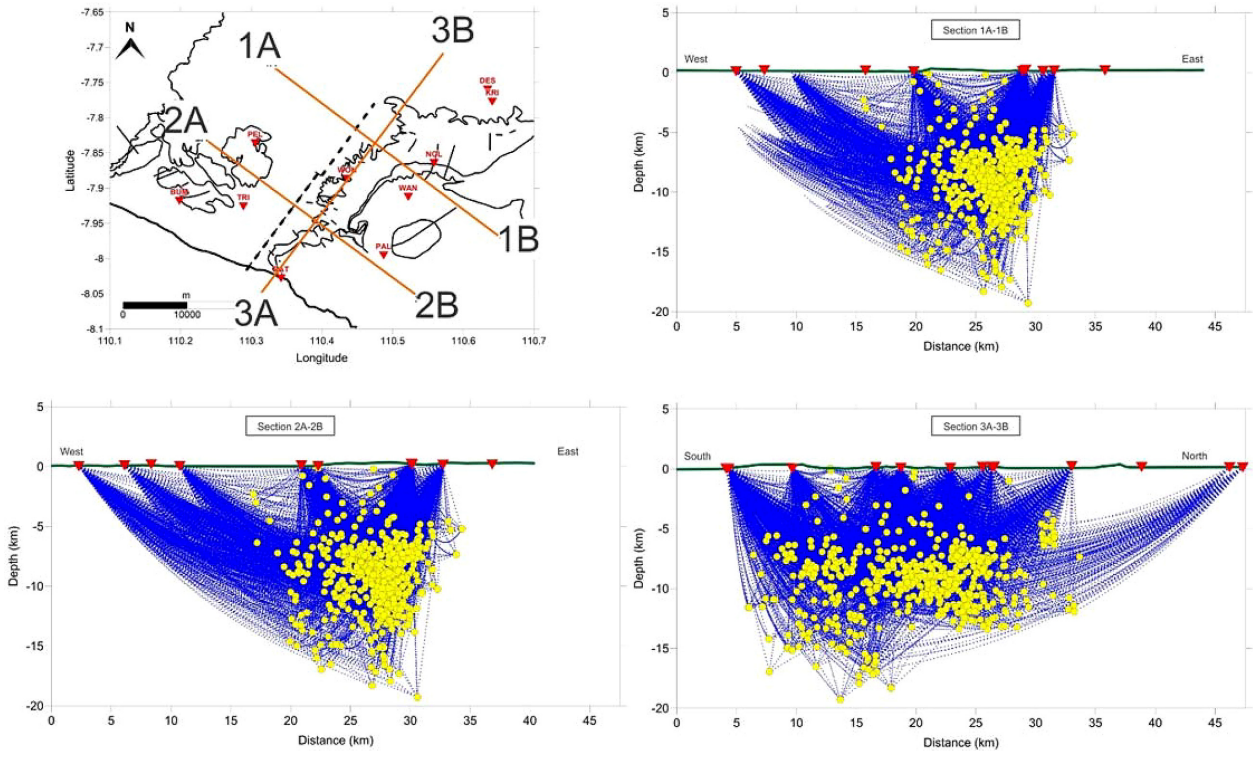

Figure 9. Ray coverage in four vertical section slices at 1A–1B, 2A–2B and 3A–3B (denoted by orange lines).

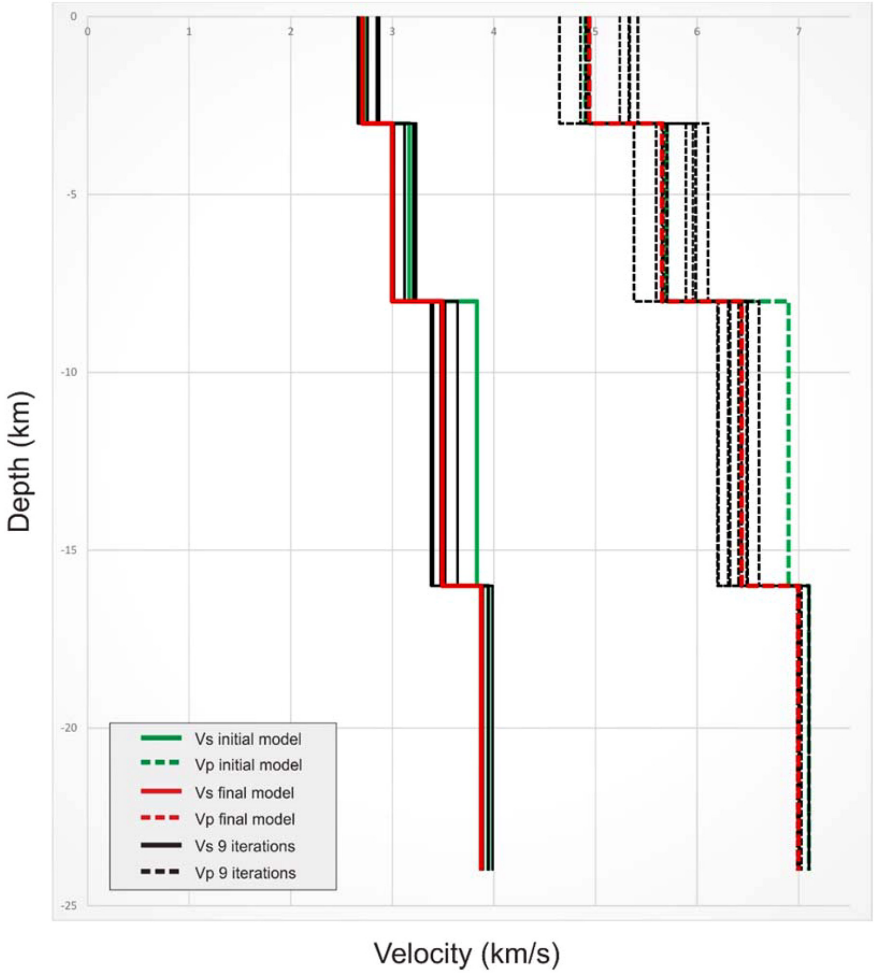

Figure 10. Results of an initial 1-D velocity model optimization after nine iterations. The initial model is shown in green, the final model as the reference velocity is shown in red and black lines show the iterative evolution through to the 9th iteration.

into tetrahedral grids joining nodes from adjacent depth levels using a quasi-continuous parameterisation. Furthermore, the matrix calculation was required in this process. Matrix calculation was constructed along the ray paths using the bending method. The effect of velocity variation at each node on the traveltime of each ray was computed numerically to represent the *P*- and *S*-velocity anomalies.

The results of the checkerboard velocity anomaly test in the study area (horizontal and vertical sections) for 10 × 10 km^2 grid size are shown in Figs 3 and 4, respectively. The ray traces passed through a medium with negative anomalies of −10 per cent (characterized by red) and positive anomalies of +10 per cent (characterized by blue) in the synthetic velocity model. A recovered synthetic model could be clearly seen in the checkerboard test tomogram results for the shallow depth slices (5 km and 10 km), as indicated by the similar patterns of blue and red colours. The tomogram successfully imaged eight blocks in the centre of the study area and exhibited similar patterns of blue and red colours between the model and the inversion result. However, the resolution decreased at greater depths (15 km), and the recovered model was less detailed, representing only two blocks of the checkerboard test located in the middle of the study area. This was related to the greater number of aftershocks located at depths of less than 10 km.

To examine a more detailed structure, we generated a smaller grid size (5 × 5 km^2) with a positive and negative anomaly synthetic model both for horizontal and vertical sections (Figs 5 and 6, respectively). The test result showed a good correlation from a slice at 5 and 10 km depth; whereas, a good correlation at slice 15 km depth only occurred at the centre of the area (shown as a white rectangular in Fig. 5). To observe the sensitivity of structure, we applied a combination of the grid size (5 × 5 km^2 and 10 × 10 km^2) to test the resulted tomogram images of the study area (Fig. 7). The whole test showed that the structure at the centre of the research area was well resolved within 5 × 5 km^2; whereas the structure at the peripheral was is well resolved within a larger grid size (10 × 10 km^2).

The ray coverage in horizontal sections of the study area is presented in Fig. 8. Blue dots indicate the ray paths of seismic waves from the hypocentres to the seismic stations. The ray coverage in deeper sections is less dense due to the sparse distribution of earthquakes located at depths of between 9 and 20 km. In the ray coverage diagrams for vertical sections shown in Fig. 9, Sections 1A–1B and 2A–2B image the subsurface perpendicular to the Opak Fault and Sections 3A–3B image the subsurface parallel to the Opak Fault.

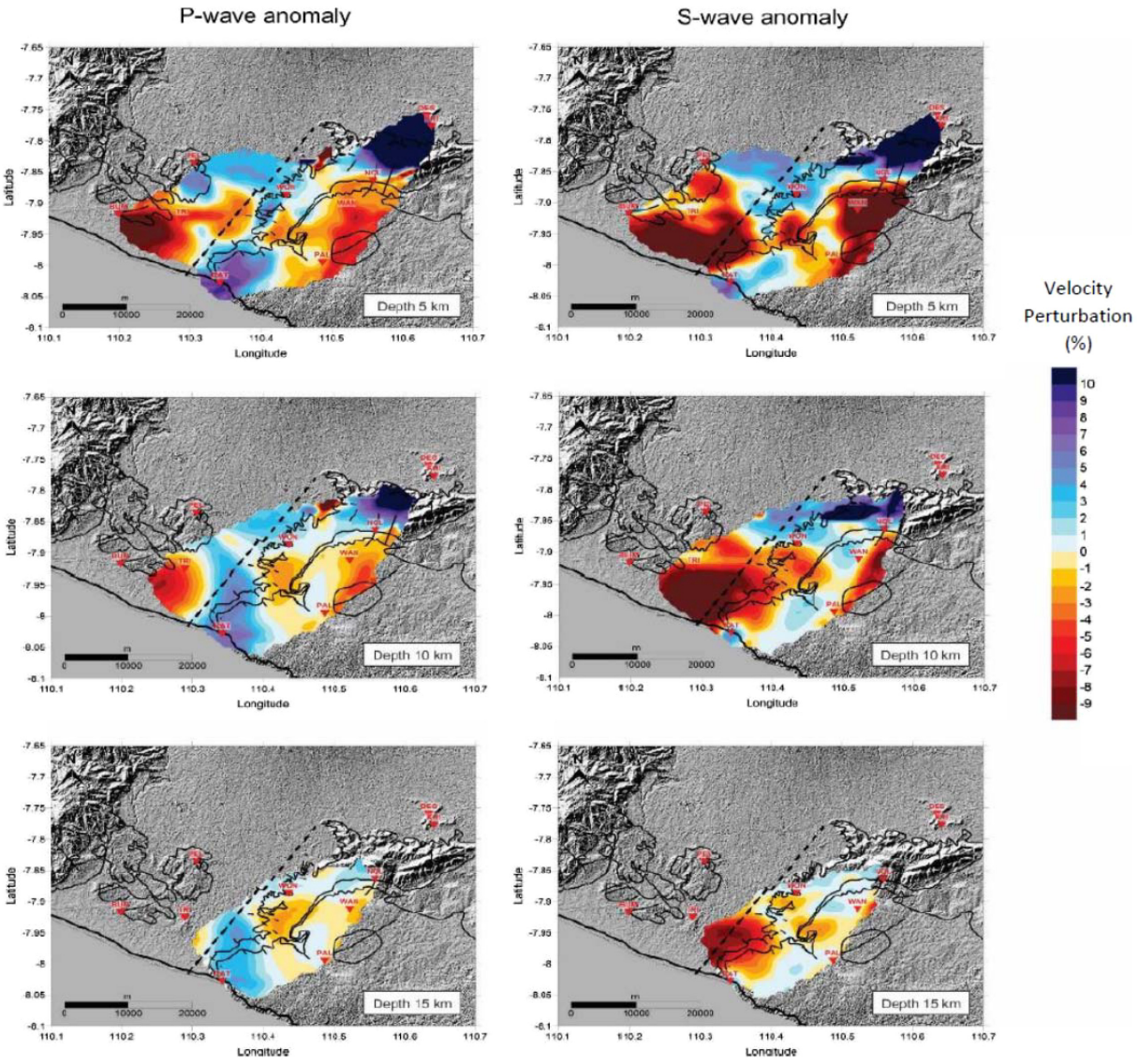

Figure 11. *P*- and *S*-wave anomaly maps in horizontal sections. The anomaly contrast between the east and west sides of the study area is interpreted as a fault.

The ray coverage resolution is very good for tomographic modelling, as our target structure was located near the centre of the ray coverage. The dense ray coverage zone had a better resolution for tomographic modelling than those the sparse ray coverage zone (Figs 8 and 9).

5 RESULT AND DISCUSSION

The calculations of 1-D velocity model as a reference in this tomography study were obtained from LOTOS-13 program using the initial model of Wagner *et al.* (2007). The procedure was performed by selecting events that were distributed as homogenously as possible over the depth. The selected events were simultaneously inverted to obtain the relocated hypocentre as well as the optimized 1-D velocity. This last procedure was similar to VELEST software (Kissling *et al.* 1994). The detailed explanation of the optimization is described in Koulakov & Sobolev (2006). The resulting tomogram image is displayed velocity perturbations in units of per cent (per cent) from this optimized velocity model (Fig. 10).

The maps of *P*- and *S*-wave anomalies in horizontal slices at various depths are shown in Fig. 11. Both the *P*- (V_P) and *S*-wave velocity (V_S) tomograms demonstrate that low-velocity anomalies are located to the east and to the southwest of the Opak Fault at 5 km depth. Positive anomalies are located to the northeast, northwest and south of the Opak Fault. At the depth of 10 km, these anomalies become weaker, and the coverage area is smaller due to the poorer ray coverage. The lowest and highest anomaly values of about −10 per cent and +10 per cent, respectively, are found southwest and east of the Opak Fault at this depth. The tomographic inversion results in the 15-km depth slices are limited since most earthquakes are located above this depth.

The tomography results are depicted in vertical sections in Fig. 12. Each slice illustrates the subsurface velocity variation both for V_P and V_S, in sections oriented perpendicular and parallel to the Opak Fault. In the *P*-wave tomogram for Sections 1A–1B and

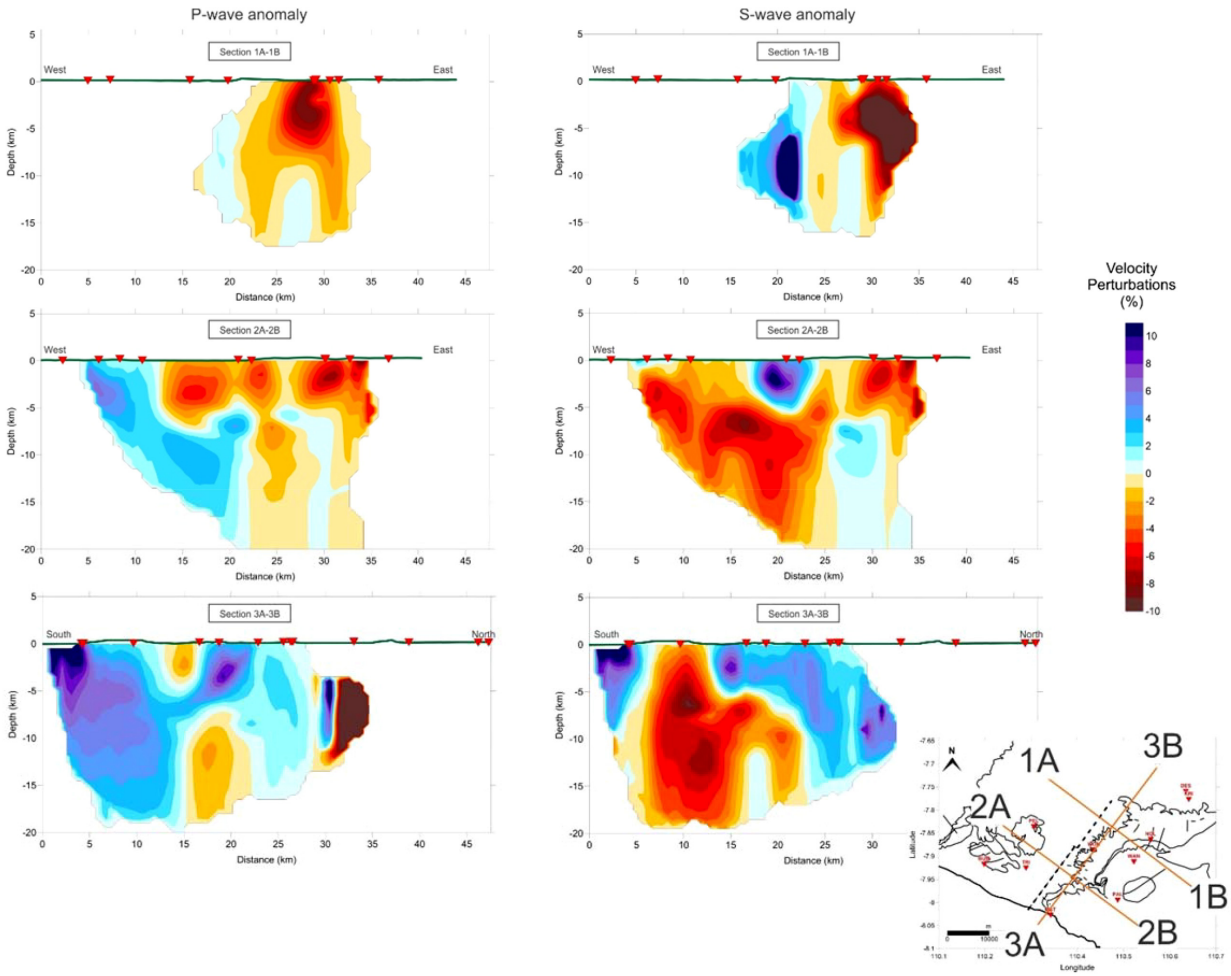

Figure 12. *P*- and *S*-wave anomaly maps in vertical sections. Negative anomalies are apparent down to 15 km depth in the vertical section. Sections 1A–1B and 2A–2B display contrasting subsurface anomalies in the right-hand and left-hand parts of each section. Sections 3A–3B exhibit a tendency toward dominantly negative anomalies rather than positive anomalies.

2A–2B, negative anomaly values are apparent up to 10 km depth in the southeastern part of the study area, while positive anomaly values occurs in the northwestern part. However, the V_S tomogram shows similar features to the V_p result in Sections 1A–1B and contrasting features in Sections 2A–2B. The differences between the *P*- and *S*-wave tomograms may be due to a high-water content in this zone that causes a large reduction in shear strength, as *S*-waves are highly sensitive to such conditions. The parallel vertical Sections 3A–3B represent anomaly maps from the southwestern to the northeastern parts of the study area. These tomograms exhibit negative anomalies up to 15 km depth. A negative anomaly is located in the southwest of the study area in Section 3A–3B, while the northeast displays a greater positive anomaly. This section is located closest to the overall spatial distribution of aftershock hypocentres of the Yogyakarta earthquake, and the area is generally dominated by a negative anomaly.

Maps of *P*- to *S*-wave velocity ratios, or V_p/V_s ratios, are shown in Fig. 13 for both horizontal and vertical sections. Greater V_p/V_s ratio values are shown in red and lower V_p/V_s ratio values are shown in blue to dark brown. Lower V_p/V_s ratios are found in the centre of the study area at shallow depths and the overall V_p/V_s ratios increase with depth and expand in the southwest. At the Opak Fault, the V_p/V_s ratio is higher than that of the surrounding area, particularly in the southwestern section. The zone of relatively high V_p/V_s ratios broadens down to 15 km depth.

In comparison, the *P*- and *S*-wave anomaly values in this high-ratio zone both exhibit dominantly negative velocity anomalies. This zone coincides with the location of a young volcanic material deposit whose high V_p/V_s ratio reflects the presence of unconsolidated rocks and it is vulnerable to earthquakes. This finding agrees with the previous study of Walter *et al.* (2008) who used micro-tremor measurements to determine that this unconsolidated material is responsible for high levels of damage in the area during the 2006 Yogyakarta earthquake.

5.1 Regional geology interpretation

Geological records of the study area (Fig. 14) indicate that the extent of the Sentolo Formation, which contains agglomerates, marl and layered limestone, correlates well with low-velocity anomaly at the depth of 5 km. The youngest rocks in the area belong to the Kepek and Wonosari Formations east of the Opak Fault and consist of 200–800 m of layered calcarenite limestone and calcarenite tuff

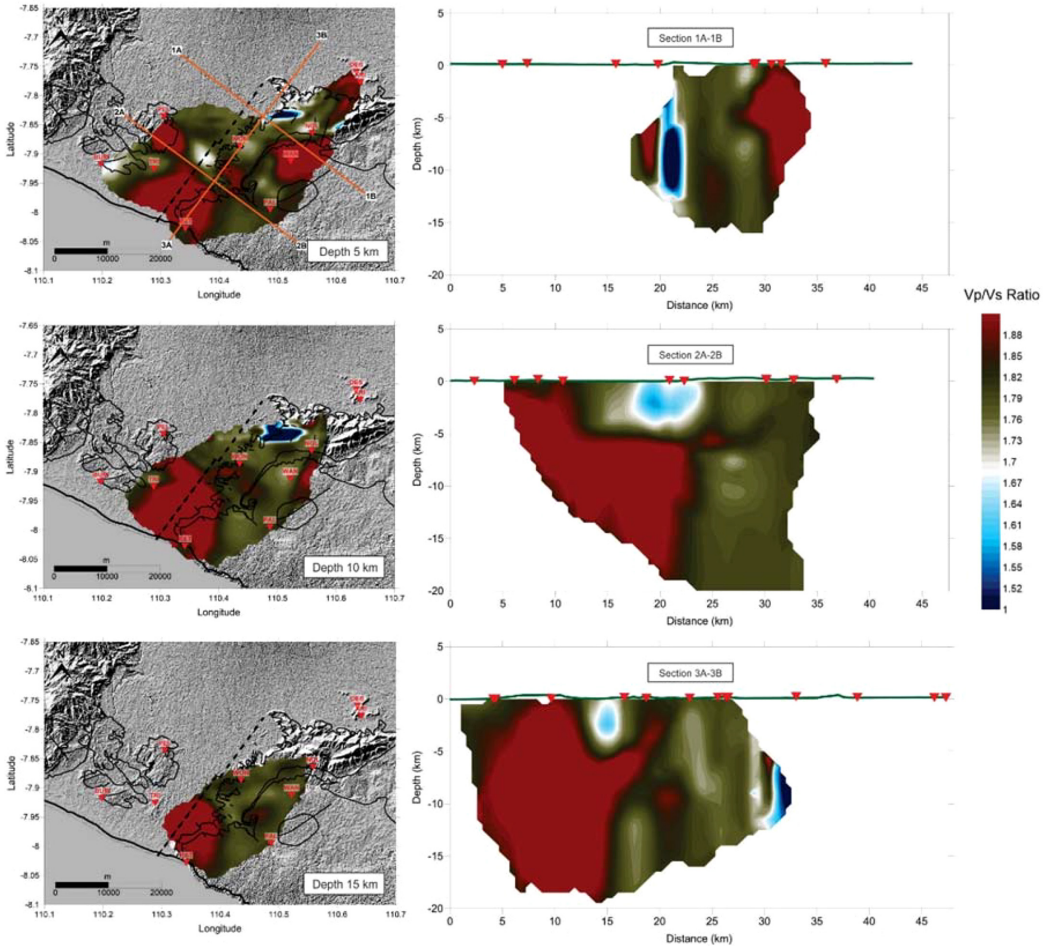

Figure 13. V_p/V_s ratio maps in horizontal and vertical sections. The highest V_p/V_s ratios are located around the area that experienced severe damage.

(Surono *et al.* 1992; Rahardjo *et al.* 1995; Sudarno 1997). The *P*-wave tomogram shows low-velocity anomaly in the location of these formations.

The largest anomalies occurred in the Nglanggran and Sambipitu Formations in the northeastern part of the study area. These formations are dominated by volcanic breccias, agglomerates and andesitic lava (Rahardjo *et al.* 1995). However, in the southwestern part of the study area, these formations were associated with negative velocity anomaly due to the present of soft sediments that were transported from the Merapi volcano as formerly erupted material.

5.2 Structural Fault Interpretation

Velocity contrasts occurs at depth in both horizontal and vertical sections, as shown in the tomogram profiles (Figs 11 and 12). The horizontal velocity contrast structure may be controlled by lithology contrast, with the high-velocity zone representing Oligo–Miocene pyroclastic & volcanic breccia members of the Kebo-Butak, Semilir and Nglanggran Fms and the low-velocity zone representing carbonate or other sedimentary rocks overlying the Oligo–Miocene volcanics. The horizontal velocity contrast is related to contacts between these rock types (i.e. volcanic and sedimentary), whereas the vertical velocity contrast may correlate with the fault zone (Fig. 11). The projection of the fault inferred from the surface location in the eastern sector loosely matches the velocity contrast surface at depth, as well as the hypocentre locations (Fig. 12). The vertical sections represented in Fig. 12 are perpendicular to the structural trend of the Opak Fault. The *S*-wave tomogram for Sections 2A–2B indicates that the negative anomaly persists at depth of 5 km, while the positive anomaly is present at depth of 20 km. A similar pattern can be found in Sections 1A–1B, in which the western part has a uniform velocity to a greater depth than in the eastern part. These observations indicates an oblique anomaly consistent with an uplifted hanging wall on the west side of a reverse fault. It can also be seen that this unnamed fault is located on the east side of the Opak Fault as described by Anggraini (2013). We assume that this unnamed fault trend is possibly associated with the extension of the NE–SW fault zone at Ngalang River (namely Ngalang Fault) as shown in Geological Map of Surakarta—Giritontro Quadrangle of Surono *et al.* (1992). The north–south profiles shown in Fig. 12 (Section 3A–B) are similar to the regional geology pattern described by Karnawati *et al.* (2006). The depression structure at the vicinity of Opak–Wonosari High area is associated with the very-low-velocity anomaly values in the tomograms, which might correspond to the filled unconsolidated sediment. The graben structure depicted in the regional geological map is supported by the very-low-velocity anomaly values in the tomograms, which may correspond to unconsolidated sediment. Therefore, this zone is potentially favourable

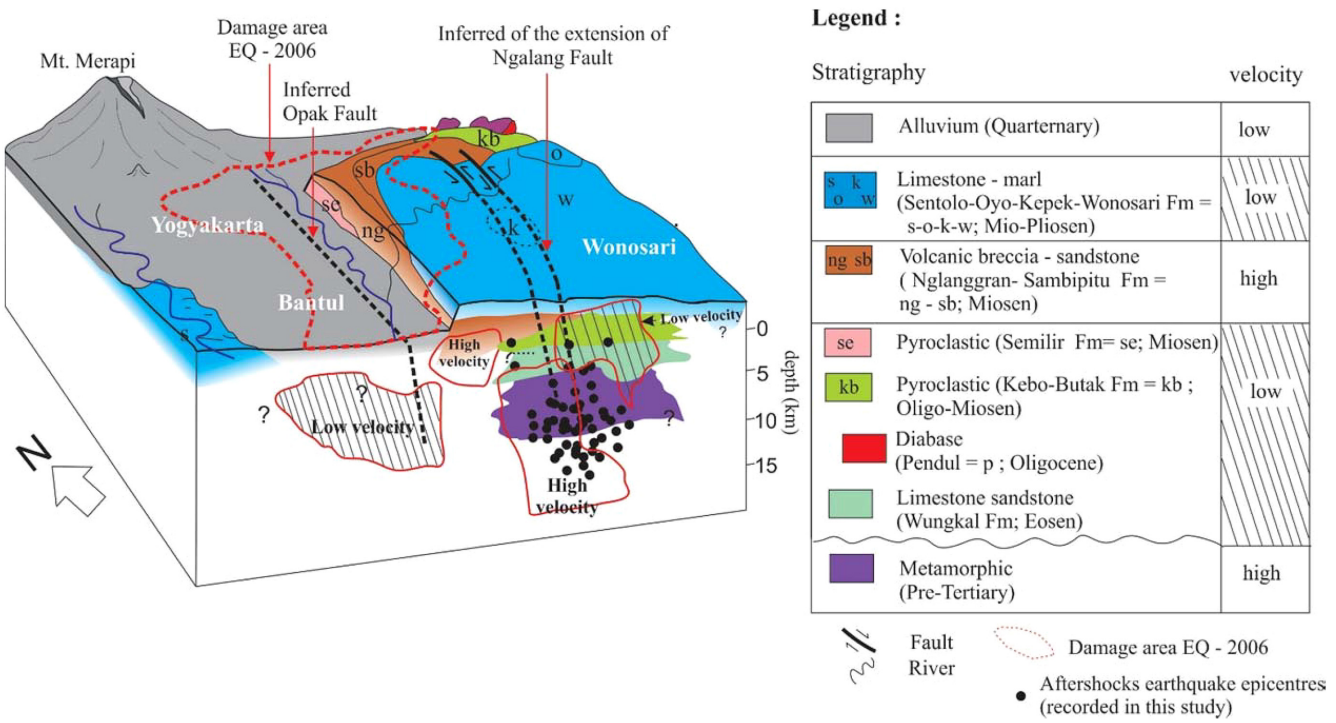

Figure 14. Sketch of Yogyakarta Tectonics framework. The sequence of metamorphic and pyroclastic rocks below the limestone (Wonosari Fm) is inferred from regional stratigraphy. Regional stratigraphic scheme is summarized from Rahardjo *et al.* (1995); Sudarno (1997) and Surono *et al.* (1992). The V_p and V_p/V_s structures derived from the tomography analysis.

to amplification of ground motion and severe damage during the earthquakes.

6 CONCLUSION

This work highlighted the structural features of NE–SW located to the east of the Opak Fault, based on a tomographic inversion, possibly related to the extension of the fault zone at the Ngalang River. This fault zone is possibly extends to the further southwest. An analysis of *P*- and *S*-wave tomograms was used to define the characteristics of the fault responsible for the Yogyakarta earthquake, with the preliminary conclusion that a strike-slip fault with a reverse component striking northeast–southwest and dipping to the east. A depression structure was also clearly observed beneath Yogyakarta in north–south-oriented vertical tomogram sections. The low-velocity anomaly in the depression area indicates the potential for severe damage due to site effects, and this area is thus susceptible to the amplification of seismic waves. Further geoscientific investigations are required to better understand the seismic hazards associated with these features in the area around Yogyakarta, Java and Indonesia.

ACKNOWLEDGEMENTS

We thank the Geophysics Laboratory of Universitas Gadjah Mada (UGM) for their support. This project is partly funded by the Ministry of Research, Technology and Higher Education Republic of Indonesia through INSINAS Batch I, contract Nr. 3216/UN1.P.III/DIT-LIT/LT/2017. Fruitful discussions with Salahuddin Husein is deeply appreciated. We thank to Stefanie Donner and an anonymous reviewer for their constructive comments.

REFERENCES

Anggraini, A., 2013. *The 26 May 2006 Yogyakarta Earthquake, Aftershocks and Interactions. Dissertation at the Faculty of Mathematisch-Naturwissenschaftlichen,* University of Potsdam, Germany.

Bohm, M. *et al.*, 2005. The MERAMEX project—a seismological network in Central Java, Indonesia, *Sonderkolloquium 'Geotechnologien',* GFZ, Potsdam, pp. 6–9.

International Recovery Platform and Universitas Gadjah Mada, 2009. *Recovery Status Report: The Yogyakarta and Central Java Earthquake 2006*. Kobe, Japan.

Karnawati, D., Pramumijoyo, S. & Hendrayana, H., 2007. Geology of Yogyakarta, Java: the dynamic volcanic arc city, *The Geological Society of London, IAEG 2006 Paper number 363,* pp. 1–7.

Kawazoe, Y. & Koketsu, K., 2010. Source fault and rupture process of the 2006 yogyakarta earthquake, AGU fall meeting abstracts, http://adsabs.harvard.edu/abs/2010AGUFM.S43A2030K.

Kissling, E, Ellsworth, W.L, Eberhard-Phillips, D & Kradolfer, U, 1994. Initial reference models in local earthquake tomography, *J. Geophys. Res.,* **99,** 19635–19646.

Koulakov, I & Sobolev, S.V, 2006. A tomographic image of Indian lithosphere break-off beneath the Pamir-Hindukush region, *Geophys. J. Int.,* **164,** 425–440.

Koulakov, I., 2009. LOTOS code for local earthquake tomographic inversion. Benchmarks for testing tomographic algorithms, *Bull. seism. Soc. Am.,* **99**(1), 194–214.

Koulakov, I., *et al.*, 2007. P and S velocity structure of the crust and the upper mantle beneath central java from local tomography inversion, *J. geophys. Res.,* **112,** B08310.

Muksin, U., Bauer, K. & Haberland, C., 2013. Seismic Vp and Vp/Vs structure of the geothermal area around Tarutung (North Sumatra, Indonesia) derived from local earthquake tomography, *J. Volc. Geotherm. Res.,* **260,** 27–42.

Prasetyadi, C., 2007. *Evolusi Tektonik Paleogen Jawa Bagian Timur*. Dissertation, Doctoral Program, Geological Engineering, Institut Teknologi Bandung, Indonesia.

Rahardjo, W.,Sukandarrumidi & Rosidi, H., 1995. *Geologic Map of the Yogyakarta Sheet, Jawa, 1:100.000,* 2 edn, Geological Research and Development Centre, Bandung.

.Soeria-Atmadja, R, Maury, R.C., Bellon, H., Pringgoprawiro, H. & Polve, M, 1994. Tertiary magmatic belts in Java, *Journal of Southeast Asian Earth Sciences,* **9,** 13–27.

Sudarno, I., 1997, Kendali Tektonik terhadap Pembentukan Struktur pada Batuan Paleogen dan Neogen di Pegunungan Selatan, Daerah Istimewa Yogyakarta dan Sekitarnya. *Master Thesis,* Geology Postgraduate Program, Institut Teknologi Bandung.

Surono, Toha, B. & Sudarno, I., 1992. *Peta Geologi Lembar Surakarta–Giritontro, Jawa*. Pusat Penelitian dan Pengembangan Geologi, Bandung.

Tsuji, T., Yamamoto, K., Matsuoka, T., Yamada, Y. & Onishi, K., 2009. Earthquake fault of the 26 May 2006 Yogyakarta earthquake. *Earth Planets Space,* **61,** e29–e32.

Um, Junho, , & Thurber, Clifford, 1987. A fast algorithm for two-point seimic ray tracing, *Bull. seism. Soc. Am.,* **77,** 972–986.

Wagner, D. *et al.*, 2007. Joint inversion of active and passive seismic data in central Java, *Geophys. J. Int.,* **170**(2), 923–932.

Walter, T. R. *et al.*, 2008. The 26 May 2006 magnitude 6.4 Yogyakarta earthquake south of Mt. Merapi volcano: did Lahar deposits amplify ground shaking and thus lead to the disaster? *Geochem. Geophys. Geosyst.,* **9**(5), 1–9.